3718 J. Med. Chem. 2010, 53, 3718–3729
DOI: 10.1021/jm100158v

Journal of Medicinal Chemistry Article

Targeting Multiple Chorismate-Utilizing Enzymes with a Single Inhibitor: Validation of a Three-Stage Design

Kristin T. Ziebart, Seth M. Dixon, Belem Avila, Mohamed H. El-Badri, Kathryn G. Guggenheim, Mark J. Kurth,* and Michael D. Toney*

Department of Chemistry, University of California, One Shields Avenue, Davis, California 95616

Received February 4, 2010

Chorismate-utilizing enzymes are attractive antimicrobial drug targets due to their absence in humans and their central role in bacterial survival and virulence. The structural and mechanistic homology of a group of these inspired the goal of discovering inhibitors that target multiple enzymes. Previously, we discovered seven inhibitors of 4-amino-4-deoxychorismate synthase (ADCS) in an on-bead, fluorescent-based screen of a 2304-member one-bead-one-compound combinatorial library. The inhibitors comprise PAYLOAD and COMBI stages, which interact with active site and surface residues, respectively, and are linked by a SPACER stage. These seven compounds, and six derivatives thereof, also inhibit two other enzymes in this family, isochorismate synthase (IS) and anthranilate synthase (AS). The best binding compound inhibits ADCS, IS, and AS with K_i values of 720, 56, and 80 μM, respectively. Inhibitors with varying SPACER lengths show the original choice of lysine to be optimal. Lastly, inhibition data confirm the PAYLOAD stage directs the inhibitors to the ADCS active site.

Antibiotic drug resistance, now a global health issue, has increased dramatically over the past several decades.[1] Rates of methicillin-resistant *Staphylococcus aureus* (MRSA[a]) infections doubled between the years 2000 and 2005. They are now the cause of more deaths in the United States than AIDS.[2] The low profitability and short functional lifetime of antibiotics has resulted in a steady decrease in research and development by industry.[1,3] As a result, only two new classes of antibiotics have been introduced since 1967: oxazolidinones (2000) and lipopeptides (2003).[4]

We have developed a streamlined approach for discovering potential antimicrobial lead compounds, entailing massively parallel, on-bead screens of one-bead-one-compound (OBOC), mass-tag-encoded combinatorial libraries with fluorescently labeled enzyme.[5] A small (2304-member), proof-of-concept, peptide-based library was designed to target a set of homologous chorismate-utilizing enzymes: 4-amino-4-deoxychorismate synthase (ADCS), isochorismate synthase (IS), anthranilate synthase (AS), and salicylate synthase (SS). ADCS, IS, AS, and SS catalyze the first committed steps in the formation of folate, enterobactin (an iron-chelating compound, i.e. siderophore), tryptophan, and mycobactin (a siderophore from *Mycobacterium tuberculosis*), respectively, in bacteria and apicomplexan parasites (Figure 1).[6]

Chorismate-utilizing enzymes are excellent antimicrobial drug targets for several reasons: (1) they catalyze the first committed step in formation of several metabolites critical for survival and/or virulence (Figure 1), (2) they are structurally and mechanistically homologous, suggesting the possibility that one drug could inhibit multiple metabolic pathways, (3) they are present only in bacteria, plants, fungi, and apicomplexan parasites (e.g., *Plasmodium, Toxoplasma,* and *Cryptosporidium*)[6] and absent in humans. Furthermore, these enzymes and metabolic pathways have not been fully exploited as drug targets. One example of successfully targeting these pathways is the sulfa drugs, which inhibit folate biosynthesis through inhibition of dihydropteroate synthase (DHPS), which occurs two steps downstream of ADCS.

The structural homology of ADCS, IS, AS, and SS, including nearly identical active site environments, inspired our goal to develop one compound that would inhibit more than one of these enzymes. The paradigm of multitarget inhibition by a single compound has been growing in popularity and acceptance in recent years.[7] This strategy has been exploited to discover treatments for conditions such as HIV-AIDS, cancer, depression, and *Mycobacterium tuberculosis* infections.[8−13] A drug that inhibits multiple enzymes would be highly desirable for its potentially increased potency, even at moderate binding affinities, due to inhibition of multiple critical metabolic pathways which would combine to slow growth. Also, the increased difficulty for development of primary resistance (i.e., mutation of the target enzymes to overcome inhibition), which would require multiple simultaneous and spontaneous mutations, makes this concept attractive. Nevertheless, alternative

*Corresponding Authors. For M.D.T.: phone, 530-754-5282; fax, 530-752-8995; E-mail, mdtoney@ucdavis.edu. For M.J.K.: phone, 530-752-8192; fax, 530-752-8995; E-mail, mjkurth@ucdavis.edu.

[a] Abbreviations: ACN, acetonitrile; ADC, 4-amino-4-deoxychorismate; ADCL, 4-amino-4-deoxychorismate lyase; ADCS, 4-amino-4-deoxychorismate synthase; AS, anthranilate synthase; DCM, dichloromethane; Dde, 1-(4,4-dimethyl-2,6-dioxocyclohexylidene)ethyl; DIC, diisopropylcarbodiimide; DHPS, dihydropteroate synthase; DIPEA, *N,N*-diisopropylethylamine; DMF, dimethylformamide; DMSO, dimethylsulfoxide; DTT, dithiothreitol; EDTA, ethylenediaminetetraacetate; ESI, electrospray ionization; Fmoc, 9H-fluoren-9-ylmethoxycarbonyl; HOBt, *n*-hydroxybenzotriazole; HPLC, high performance liquid chromatography; HRMS, high resolution mass spectrometry; IPTG, β-isopropylthiogalactoside; IS, isochorismate synthase; LB, luria-bertani broth; LDH, lactate dehydrogenase; MBHA, 4-methylbenzhydrylamine; MRSA, methicillin-resistant *Staphylococcus aureus*; NADH, nicotinamide adenine dinucleotide, reduced form; OBOC, one-bead one-compound; PLP, pyridoxal-5′-phosphate; SDS-PAGE, sodium dodecyl sulfate polyacrylamide gel electrophoresis; TEA, triethanolamine; TFA, trifluoroacetic acid; TIS, triisopropylsilane

 Published on Web 04/01/2010

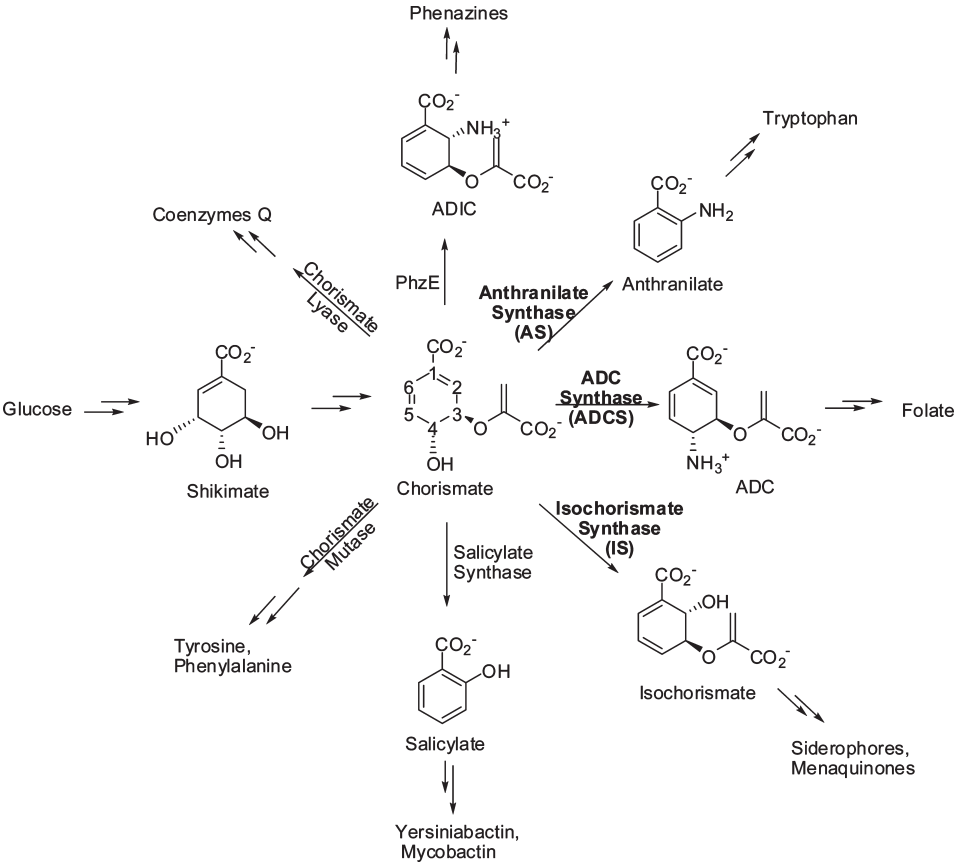

Figure 1. Chorismate is a central branch-point compound in bacterial, plant, fungal, and apicomplexan parasite metabolism. Chorismate-utilizing enzymes are essential for survival and/or virulence in these organisms. The enzymes in bold (ADCS, AS, and IS) are the subject of this work.

resistance mechanisms (e.g., efflux pumps or covalent modifications) would remain problematic.

Our inhibitor design, inspired by the popular cholesterol-lowering statin drugs, incorporates three "stages": PAYLOAD, SPACER, and COMBI, as illustrated in Figure 2. The PAYLOAD is a chorismate mimic, designed to guide the compound to the enzyme's active site. The SPACER links PAYLOAD and COMBI stages together and extends out of the active site to the solvent-exposed surface region of the proteins. The COMBI stage is where combinatorial diversity elements are introduced to the library. Schreiber and co-workers first introduced the concept of biased combinatorial libraries and used this technique to discover ligands for the SH3 domain of phosphatidylinositol 3-kinase[14] and, later, for histone deacetylases.[15]

This strategy is similar to the fragment-based drug discovery paradigm, where subcomponents of the final inhibitor are identified and optimized individually, then connected in a later stage. The fragment-based approach has the recognized disadvantage that the process of connecting fragments can be problematic.[16] In contrast, the method employed here addresses this major hurdle by connecting the fragments from the outset. Importantly, it is enabled by the massively parallel OBOC library screening and hit identification technology utilized in our approach.

In previous work, OBOC library screening employing ADCS in hit selection led to the identification and kinetic characterization of seven ADCS inhibitors.[5] The results presented therein established the efficacy of our general paradigm for chorismate-utilizing enzyme inhibition based on combinatorial chemistry and a staged inhibitor design. We further demonstrate here that the COMBI stage interacts with surface

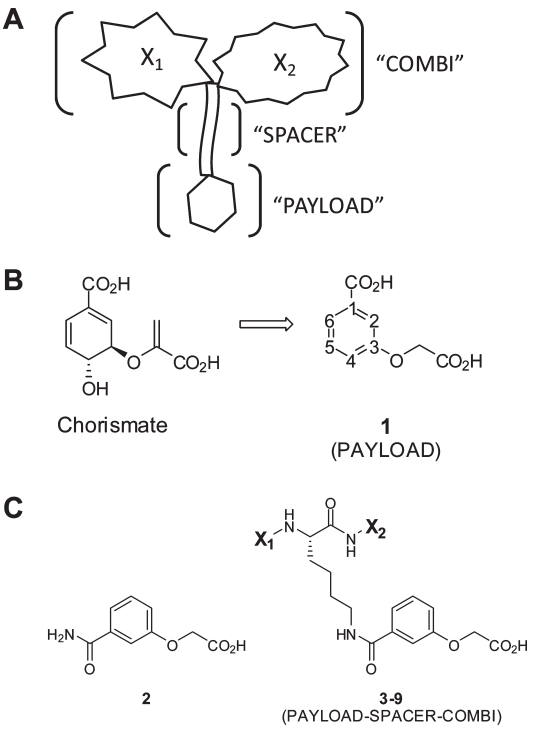

Figure 2. (A) Inhibitor design strategy employs three "stages": PAYLOAD, SPACER, and COMBI. X_1 and X_2 represent the two diversity elements present in each member of the combinatorial library. (B) PAYLOAD compound **1** is a chorismate mimic, designed to guide the inhibitors to the active site. (C) **2** was synthesized and assayed in order to compare directly the inhibition results of the fully elaborated inhibitors **3**−**9** with the PAYLOAD (for description of X_1 and X_2, see Figure 6).

Scheme 1

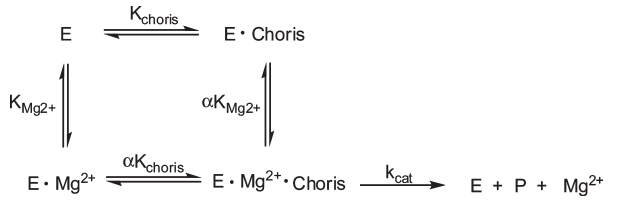

residues proximal to the active site and leads to an increased binding affinity to the enzymes. In this work, our central objective, inhibiting more than one enzyme with the same compound, is demonstrated. The seven inhibitors discovered in the ADCS screen, as well as six derivatives thereof, were assayed against IS and AS; these and other results are presented herein. Generally, the inhibitors previously characterized with ADCS bind more tightly to IS and AS. Five of the inhibitors display micromolar inhibition of ADCS, IS, and AS, and the best overall binding compound inhibits ADCS, IS, and AS with K_i values of 720, 56, and 80 μM, respectively.

Additionally, the present work investigates two important design features via synthesis and assay of four new compounds against ADCS, IS, and AS. First, the optimal length of the SPACER stage was tested by varying its length. Second, the possibility of the COMBI stage being principally responsible for the inhibition results was probed by synthesis and assay of COMBI-only and COMBI-SPACER-only compounds. These were found to inhibit minimally and nonspecifically AS and ADCS, thus verifying that all three stages are necessary for optimal inhibition.

Lastly, the inhibition results are presented in the context of the kinetic and structural properties of ADCS, IS, and AS, which are Mg^{2+}-dependent enzymes. The kinetic mechanisms employed by these enzymes explain and account for the observed inhibition patterns with respect to chorismate and the Mg^{2+} cofactor.

Results and Discussion

Kinetic Mechanisms of AS and IS. Initial rates of reactions where chorismate and Mg^{2+} concentrations were varied across wide ranges were measured. Double reciprocal plots of the kinetic data for AS and IS are shown in Figures 3 and 4, respectively. Both the AS and IS data sets were globally best-fit to eq 1, which describes a random kinetic mechanism.

$$v_i = \left\{V_{max}[\text{chorismate}][Mg^{2+}]\right\} \Big/ \left\{K_{\text{chorismate}}K_{Mg^{2+}} + \alpha K_{\text{chorismate}}[Mg^{2+}] + \alpha K_{Mg^{2+}}[\text{chorismate}] + [\text{chorismate}][Mg^{2+}]\right\} \quad (1)$$

Scheme 1 describes the equilibria and kinetic parameters that correspond to eq 1. The binding constant values for chorismate and Mg^{2+} were determined from nonlinear regression analysis and are listed in Table 1. The ADCS kinetic mechanism and substrate binding constant values were described previously;[5] those results are listed in Table 1 for comparison with AS and IS.

Table 1. Substrate Binding Constants for ADCS, IS, and AS

	ADCS[a]	IS	AS
$K_{m,}$ chorismate (μM) (saturating [Mg^{2+}])	13 ± 1	16 ± 1	3.9 ± 0.2
kinetic mechanism	ordered, chorismate binds first	random	random
$K_{\text{chorismate}}$ (μM)[b]	2200 ± 1100	3030 ± 540	25.22 ± 0.02
$\alpha K_{\text{chorismate}}$ (μM)[c]	N/A[d]	29 ± 4	14.87 ± 0.01
K_{Mg2+} (μM)[e]	5 ± 2[f]	259 ± 46	415.1 ± 0.5
αK_{Mg2+} (μM)[g]	N/A[d]	2.5 ± 0.4	244.7 ± 0.3

[a] Data taken from ref 5. [b] Reflects the binding of chorismate to the free enzyme. [c] Reflects the binding of chorismate to the [E·Mg^{2+}] complex. In principle, this is the same as the chorismate K_M in the presence of saturating Mg^{2+}. [d] Not applicable when an ordered kinetic mechanism is employed. [e] Reflects the binding of Mg^{2+} to the free enzyme. [f] ADCS value reflects the binding of Mg^{2+} to the [E·chorismate] complex. [g] Reflects the binding of Mg^{2+} to the [E·chorismate] complex.

The affinity of IS for chorismate is very low in the absence of Mg^{2+}, as reflected by the high $K_{\text{chorismate}}$ values relative to $\alpha K_{\text{chorismate}}$. This contrasts with the 1.7-fold difference between the AS values for $K_{\text{chorismate}}$ and $\alpha K_{\text{chorismate}}$. Here, α is a proportionality constant that defines the extent to which binding of one substrate is enhanced if the other is already bound. If $\alpha = 1$, binding of one substrate has no effect on the other. In IS reactions, $\alpha = 0.025$; therefore, chorismate and Mg^{2+} binding is highly cooperative. Conversely, AS has an α value of 0.59, which indicates that binding of either substrate to the free enzyme is much less dependent on the presence of the other compared to IS and ADCS.

The random kinetic mechanism employed by AS and IS contrasts with the ordered kinetic mechanism observed for ADCS.[5] In the case of ADCS, chorismate binds first, followed by magnesium. Chorismate binding to ADCS elicits a large conformational change. In support of this, substantial differences exist between the "open" and "closed" forms of ADCS X-ray crystal structures.[17] Three glutamate residues, Glu302, Glu436, and Glu439 (ADCS numbering used throughout), located just above the putative chorismate binding site, are strictly conserved among ADCS, AS, and IS, and they are proposed to coordinate Mg^{2+}. The distance between two of them, Glu302 and Glu439, reflects the extent of protein movement between open (25.3 Å) and closed (6.2 Å) forms of ADCS (Figure 5). Because the Mg^{2+} binding site is not fully formed in the "open" structure, a random kinetic mechanism is not possible for ADCS.

Conversely, AS and IS undergo a smaller conformational change on chorismate binding. This is supported by crystallographic data.[18−20] In the case of AS, one can compare the structural differences between "closed" *Serratia marcescens* AS,[18] solved with Mg^{2+} and benzoate present, and "open" *Salmonella typhimurium* AS,[19] which has no bound ligands. (These two AS isozymes are nearly identical proteins). The distance between Glu302 and Glu439 in the open and closed forms changes from 10.7 to 6.8 Å, respectively. The change in distance between these analogous glutamate residues in IS is of a similar magnitude: 9.9 Å (open) versus 5.9 Å (closed). Figure 5 depicts the open and closed crystal structures of AS and IS. Here, the MenF isochorismate synthase crystal structures were consulted[20] because structural data is not yet available for the EntC IS protein that is the subject of kinetic analyses in this work. MenF IS shares 24% sequence identity and 41%

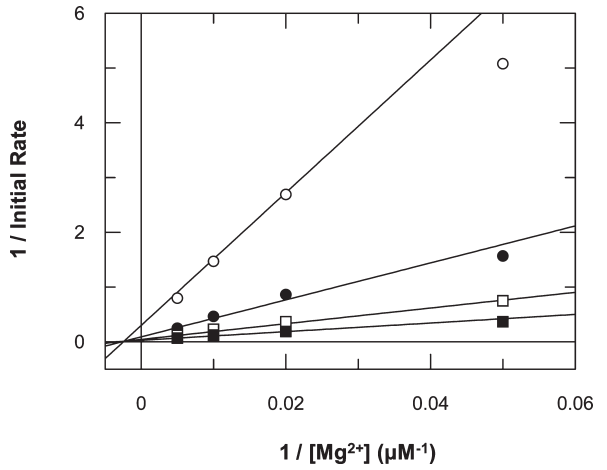

Figure 3. Double reciprocal plot of Mg^{2+} dependence indicates AS employs an equilibrium random kinetic mechanism. The concentrations of chorismate are: 1 (○), 4 (●), 12 (□), 36 (■) μM.

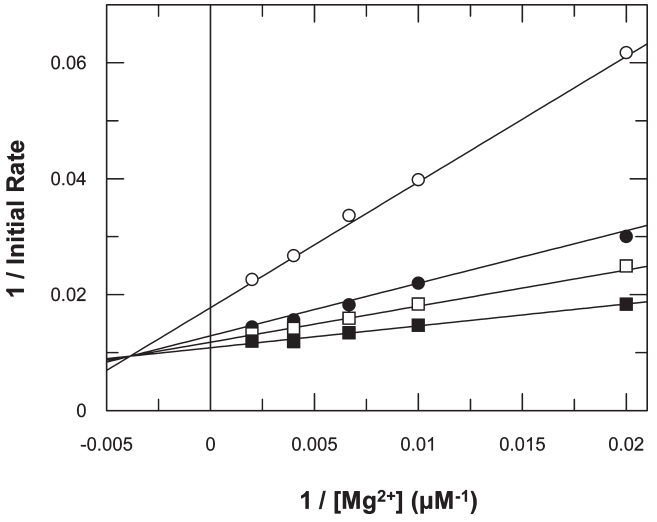

Figure 4. Double reciprocal plot of Mg^{2+} dependence indicates an equilibrium random kinetic mechanism for IS. The concentrations of chorismate are: 33 (○), 80 (●), 120 (□), 200 (■) μM.

homology with EntC IS. Further, MenF has been reported to employ a random kinetic mechanism.[21]

Because the magnesium binding site in AS and IS is more fully formed in the absence of chorismate, it is possible for the two substrates to bind independently of each other. Together, the AS and IS structural and kinetic data support a mechanism in which chorismate and Mg^{2+} bind proximal to one another in a cooperative manner. The inhibition data for ADCS, AS, and IS further support this conclusion (vide infra).

Inhibition Results. Inhibitors (**3**−**9**) identified from the ADCS on-bead screen were resynthesized[5] and assayed against IS and AS (Figure 6). The results of those assays, along with data for compounds **1** and **2**, are presented in Table 2. Remarkably, all of the inhibitors except **8** bind more tightly to IS and AS than they do ADCS, even though ADCS binding was employed in the initial bead screening binding assay. The best inhibitor of IS is **7** with a K_i value of 56 μM; the tightest binding inhibitor of AS is **5** with a K_i value of 20 μM.

The K_i values in Table 2 are for inhibition against chorismate. They were obtained from a global fit of data

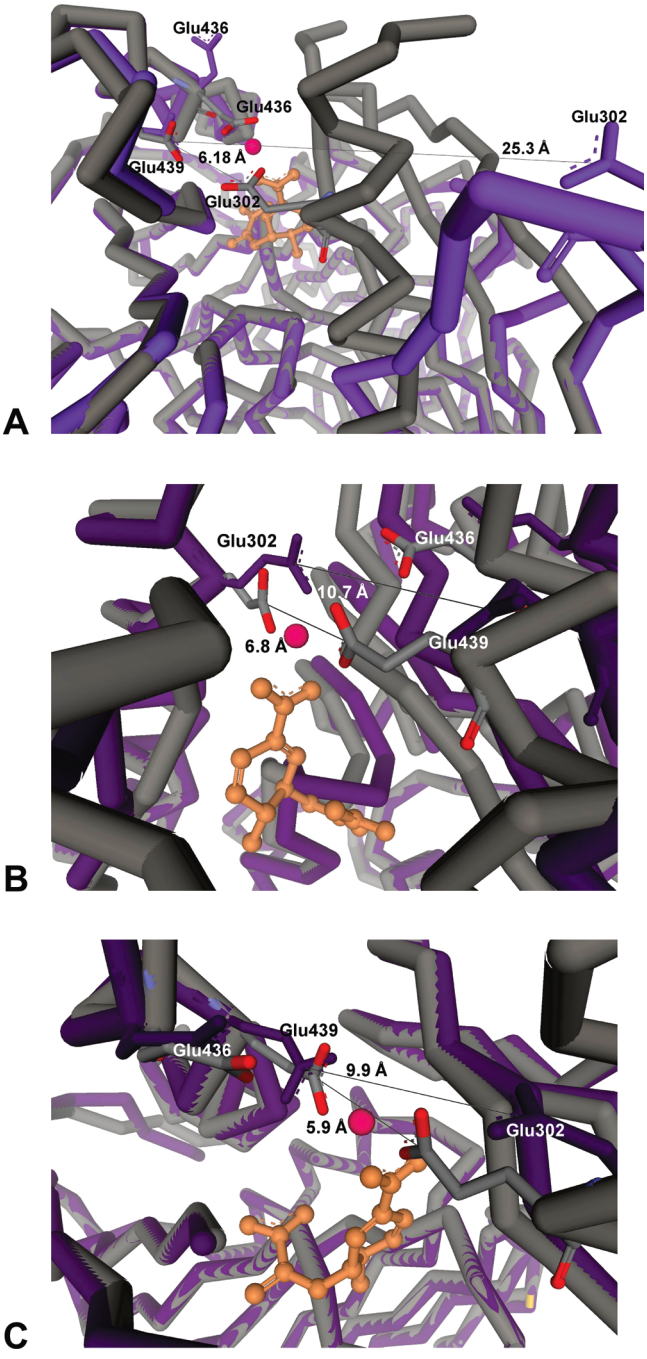

Figure 5. Overlay of open and closed X-ray structures for ADCS (A), AS (B), and IS (C). Each protein's C-α backbone is displayed in stick form with the relevant glutamic acid residues labeled and side chains rendered in sick form (Glu302, Glu436, Glu439; ADCS numbering used throughout). The gray trace represents the closed (i.e., substrate bound) structure; glutamic acid residues are colored gray. The purple trace represents the open (i.e., apo) structure; glutamic acid residues are colored purple. Chorismate (peach-colored) and Mg^{2+} (magenta) were docked into the active site of each structure.

where initial rates of reactions were measured across a wide range of inhibitor and chorismate concentrations with saturating magnesium. To assess the pattern of inhibition with respect to magnesium, the same type of analysis was performed for reactions in which chorismate was held constant at a saturating concentration and magnesium concentrations were varied from 5 to

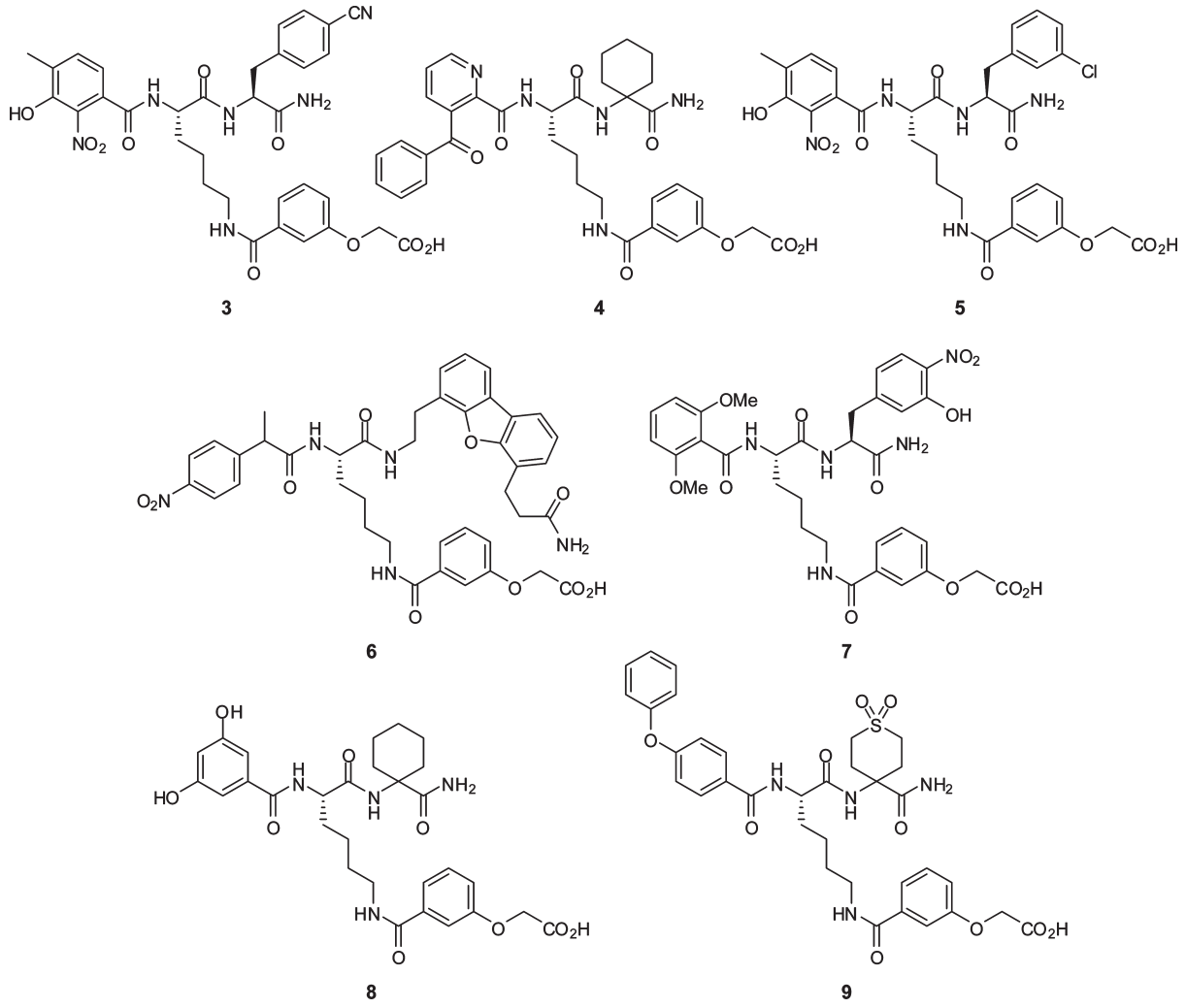

Figure 6. Structures of the compounds identified from the ADCS bead screen assay. These inhibitors were subsequently assayed against AS and IS.

Table 2. Inhibition of ADCS, IS, and AS by Library Compounds Identified in an ADCS On-Bead Screen

	K_i (μM)[a]			
compd	ADCS[b]	IS	AS[c]	
1	37000 ± 4000	1300 ± 100	210 ± 18	550 ± 83
2	32000 ± 2000	2600 ± 210	760 ± 6	2600 ± 300
3	540 ± 60	260 ± 21	28 ± 7	81 ± 20
4	3900 ± 500	430 ± 64	490 ± 73	1081 ± 117
5	770 ± 60	210 ± 29	20 ± 2	54 ± 4
6	360 ± 30	190 ± 19	250 ± 61	110 ± 7
7	720 ± 60	56 ± 3	80 ± 2	N/A[d]
8	1100 ± 100	1200 ± 99	160 ± 16	389 ± 24
9	710 ± 80	170 ± 11	570 ± 44	1020 ± 59
inhibition vs chorismate	competitive	competitive	mixed	
inhibition vs Mg^{2+}	competitive	noncompetitive	competitive	

[a] Inhibition constants reflect inhibition with respect to chorismate binding. [b] Data taken from ref 5. [c] K_i' values, listed in the last column, reflect the inhibitor binding to the [E·chorismate] complex. [d] Not applicable because compound 7 exhibited pure noncompetitive inhibition with respect to chorismate.

500 μM. Representative plots of inhibition with respect to each substrate for AS and IS are shown in Figures 7 and 8, respectively.

The most appropriate comparison of inhibition by fully staged inhibitors **3**−**9** to inhibition by the PAYLOAD alone is with amide derivative **2** because the SPACER and PAYLOAD stages are connected by an amide bond. The inhibition of IS by fully elaborated **7** is 46-fold tighter than **2**, and compound **5** binds 38-fold more tightly to AS than **2**. Compared to ADCS, inhibitors **3**−**9** overall bind more tightly to AS and IS; however, the degree to which the COMBI stage improves inhibition is generally less for IS and AS than ADCS. The K_i value of the best inhibitor of ADCS, **6**, is 360 μM, which is an 89-fold improvement relative to **2**. The greater impact of the COMBI stage on ADCS binding may be related to the larger conformational change that occurs on chorismate binding, relative to IS and AS.

With AS, the lack of competitive inhibition versus chorismate was unexpected. None of the compounds competitively inhibits chorismate binding; **1**−**6**, **8**, and **9** display mixed inhibition and **7** is a noncompetitive inhibitor. Given the similarity between chorismate and **1** and **2**, one would expect these inhibitors to be competitive against chorismate. The K_i' values listed in Table 2 reflect the binding of inhibitor to the [AS·chorismate] complex. Except for compound **6**, the inhibitors bind more tightly to the free enzyme than to the [AS·chorismate] complex. The average of the K_i'/K_i ratios

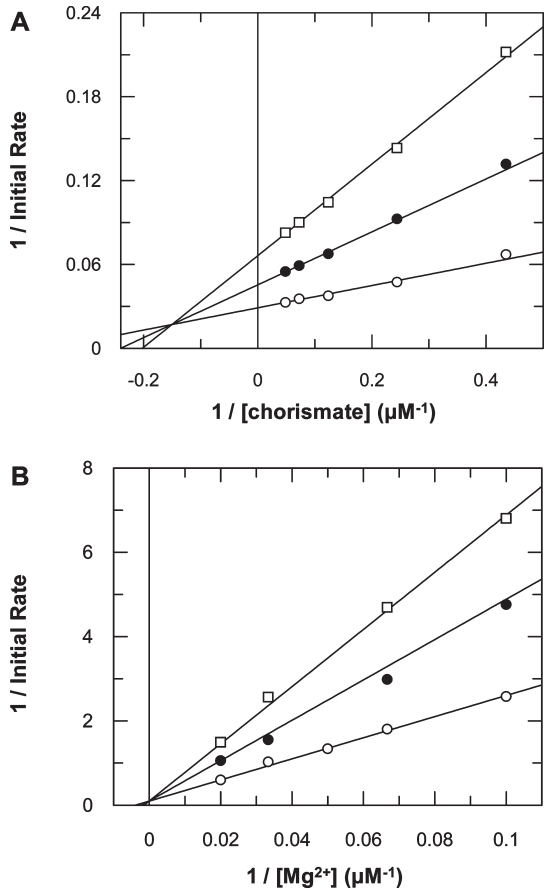

Figure 7. (A) AS inhibition by **8** with respect to chorismate. Concentrations of **8** are 0 (○), 220 (●), 500 (□) μM. (B) AS inhibition by **8** with respect to Mg^{2+}. Concentrations of **8** are 0 (○), 200 (●), 375 (□) μM.

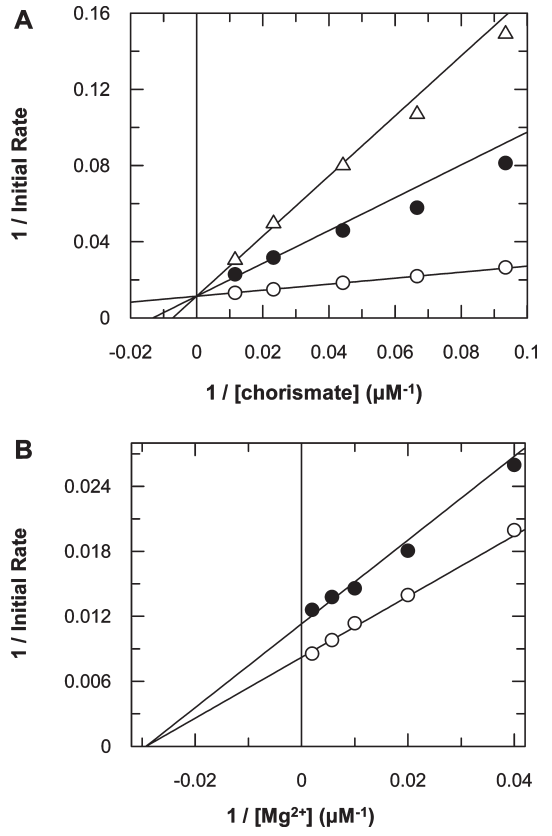

Figure 8. (A) IS inhibition by **7** with respect to chorismate. Concentrations of **7** are 0 (○), 250 (●), 500 (□) μM. (B) IS inhibition by **7** with respect to Mg^{2+}. Concentrations of **8** are 0 (○), 250 (●) μM.

Scheme 2

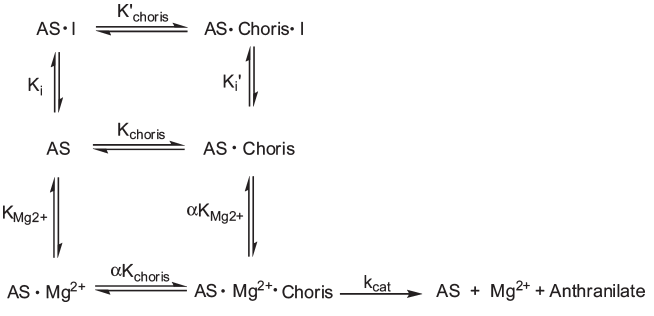

among those inhibitors is 2.5. Scheme 2 depicts the set of equilibria that describe noncompetitive and mixed inhibition patterns; it additionally takes into account the random kinetic mechanism of AS. For pure noncompetitive inhibitors, $K_i' = K_i$; for mixed inhibition, $K_i' \neq K_i$.

Additionally, the inhibition data for PAYLOAD **1** were plotted as a Dixon plot (i.e., $1/v_i$ vs [**1**]) for several chorismate concentrations (Figure 9). A linear Dixon plot rules out the possibility of other inhibition scenarios, such as partial inhibition and other types of mixed inhibition, because these inhibition modes would result in a curved Dixon plot. It also indicates that the [AS·chorismate· inhibitor] complex is catalytically inactive.[22] The linearity of the data in Figure 9 confirms Scheme 2 as an accurate description of AS inhibition by **1**, and by extension, **2**−**5**, **8**, and **9**. Because of limited amounts of these compounds, there is not a sufficient number of data points to construct analogous Dixon plots for **2**−**5**, **8**, and **9**. However, it is assumed that these inhibitors follow the same inhibition pattern as **1** based on the similar K_i'/K_i ratios observed for compounds **1**−**5**, **8**, and **9**.

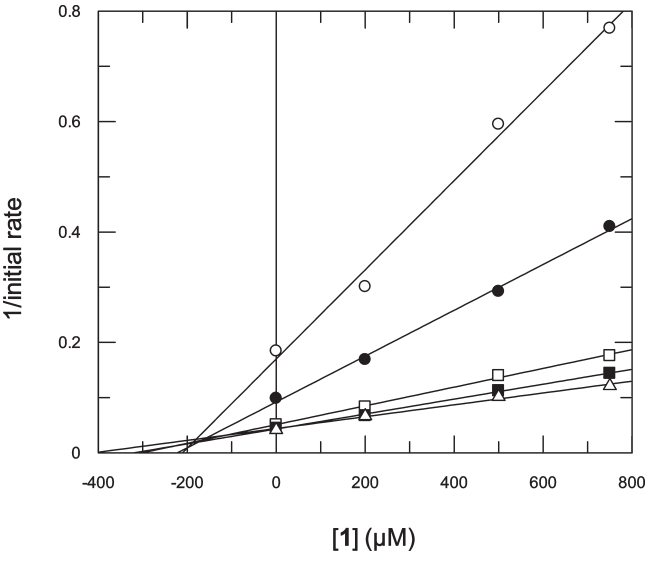

Figure 9. Dixon plot of AS inhibition by **1**. Linear regression yields an R value of >0.99 for each chorismate concentration, indicating that the [AS·chorismate·**1**] complex is catalytically inactive. The concentrations of chorismate are: 2.1 (○), 4.1 (●), 8 (□), 10 (■), 20 (△) μM.

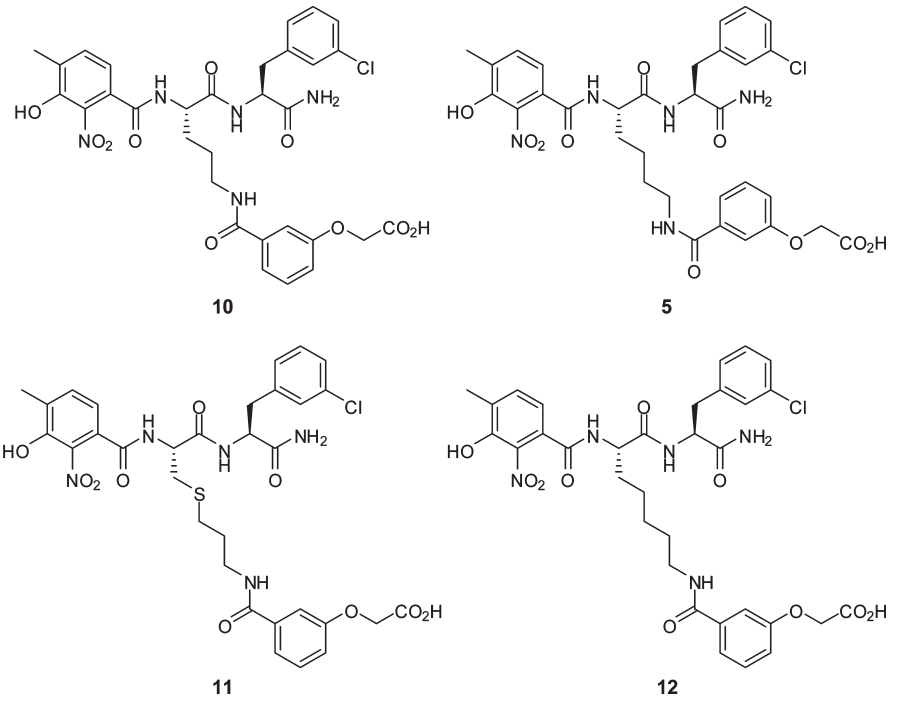

Figure 10. Compounds **10**, **5**, **11**, and **12** comprise different SPACER elements: L-ornithine, L-lysine, *S*-propyl-L-cysteine, and L-α-homolysine, respectively. These compounds are composed of identical PAYLOAD and COMBI moieties.

The competitive inhibition with respect to Mg^{2+} reveals that these compounds are binding near the AS active site. (This result also confirms that the [AS·chorismate·inhibitor] complex is catalytically inactive because Mg^{2+} is required for catalysis). The X-ray crystal structure of *S. marcescens* AS, a nearly identical homologue of the *S. typhimurium* AS under study here, was solved in the presence of magnesium.[18] In this structure, magnesium is positioned in the active site immediately proximal to the C1 carboxylate group of the chorismate analogue benzoic acid. Additionally, three glutamate residues surround and coordinate Mg^{2+}. The inhibitors likely bind near the analogous glutamate residues to competitively inhibit Mg^{2+} from binding. To propose the precise inhibitor binding location to AS would be speculative. Therefore, one must evaluate all subsequent inhibition data in light of this uncertainty.

Conversely, in the IS inhibition studies, each inhibitor competitively inhibited chorismate and noncompetitively inhibited magnesium. The different inhibition patterns with respect to each substrate are a consequence of the random kinetic mechanism employed by IS and AS. Separate, adjacent binding sites exist for chorismate and Mg^{2+}, and the inhibitors bind to only one of these locations, allowing the other substrate to bind.

Optimal SPACER Length. Lysine was originally chosen as the SPACER element for our discovery library after docking studies with the ADCS crystal structure[17] indicated its 4-carbon side chain is an optimal length. To test this deduction, compounds **10** and **11** were synthesized and assayed against ADCS, IS, and AS (Figure 10). Analogue **10** was prepared with L-ornithine, such that the SPACER contains one fewer carbon relative to lysine. Because of the high cost and limited availability of a L-α-homolysine precursor, **11** (an isosteric analogue of **12**) was instead synthesized (Figure 11).

The inhibition constants obtained from kinetic assay of **5**, **10**, and **11** are listed in Table 3. SPACER lengths correspond to the distance between the amide carbonyl carbon of the PAYLOAD and the α-carbon of the amino acid (e.g., ornithine, lysine, cysteine) with its side chain in the extended conformation. The K_i values reflect inhibition against chorismate. Determination of the inhibition mechanism (i.e., competitive versus noncompetitive) followed a process similar to that described for inhibitors **3**–**9**.

AS and ADCS are most sensitive to SPACER length. A shorter SPACER strongly decreases binding to ADCS, and a longer SPACER is most detrimental to AS binding. However, it is difficult to interpret the effect of SPACER length on AS inhibition because these compounds are not competitive inhibitors of chorismate (vide supra). IS was the least sensitive to the SPACER length; the difference in inhibition by **5**, **10**, and **11** was minimal. Despite a small improvement in inhibition of IS by a longer SPACER (**11**), this benefit does not counterbalance the cost paid with ADCS for the longer SPACER. The results in Table 3 support the deduction from the crystal structure that lysine provides the optimal SPACER length for ADCS inhibitors.

Validation of PAYLOAD-Directed Active Site Binding. The inhibitor design strategy is based on two principles: (1) the PAYLOAD directs these compounds to the active site, and (2) synergistic PAYLOAD and COMBI interactions strengthen enzyme binding. PAYLOAD-deleted compounds **14** and **15** (Figure 12) were synthesized and assayed against ADCS, IS, and AS to test the possibility that inhibition of these two enzymes is mainly due to COMBI interactions with surface residues. K_i values are listed in Table 4. The results show that inhibition is best when all three stages (PAYLOAD, SPACER, COMBI) are present. Furthermore, inhibition of ADCS and AS by **14** and **15** is noncompetitive against both substrates, indicating that the two substrates and the inhibitor can bind simultaneously to the enzyme and that the inhibitor is not binding to the active site. One must interpret the AS inhibition data with caution. For AS, the results in Table 4 indicate that the PAYLOAD directs

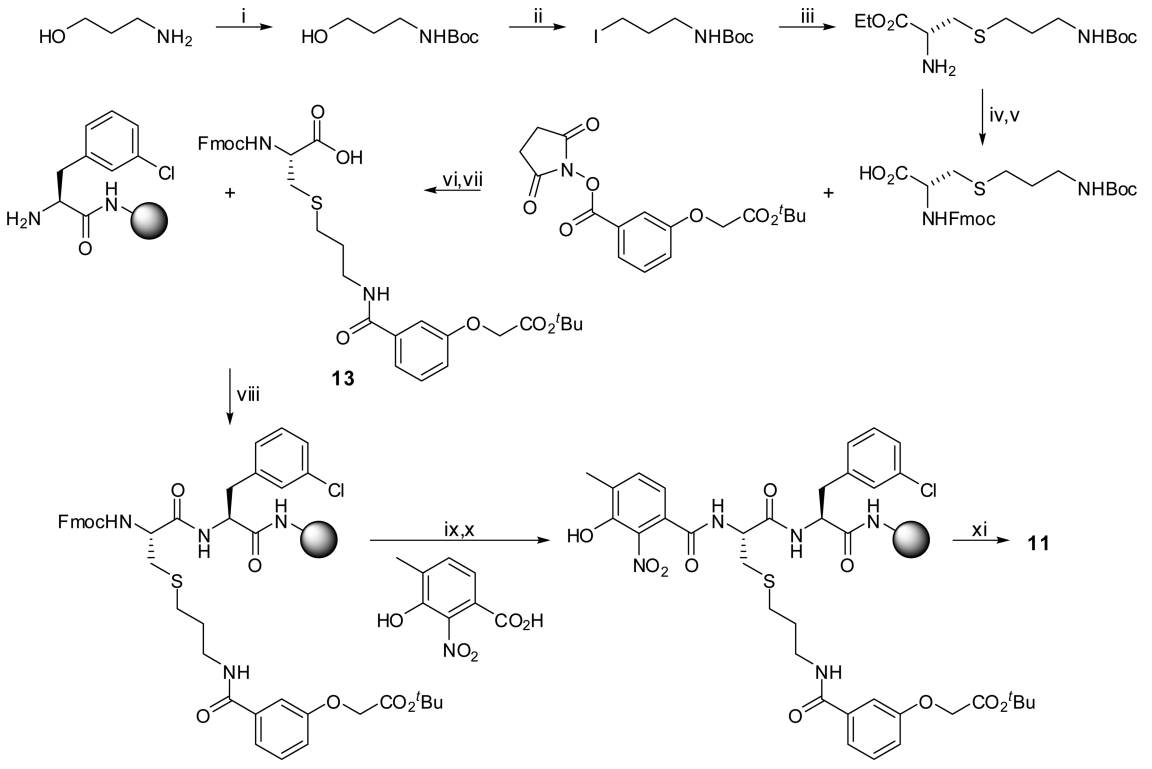

Figure 11. Synthesis of compound **11**. Reagents and conditions: (i) Boc_2O, Et_3N, DCM, reflux, overnight; (ii) I_2, PPh_3, 1*H*-imidazole, DCM, rt, 3.5 h; (iii) Cs_2CO_3, DMF, methylester of L-cysteine hydrochloride, rt, overnight; (iv) LiOH, MeOH, rt, 2 h; (v) Fmoc-OSu, THF, Na_2CO_3, 0 °C, 1 h; (vi) TFA:DCM (3:7), rt, 30 min; (vii) DIPEA, H_2O/ACN, rt, 7 h; (viii) HOBt, DIC; (ix) 20% piperidine in DMF, 2 × 10 min; (x) HOBt, DIC; (xi) TFA/H_2O/TIS (95, 2.5, 2.5, v/v/v).

Table 3. The Effect of SPACER Length on Inhibition of ADCS, IS, and AS

		K_i (μM)[a]		
inhibitor	SPACER length (Å)	ADCS[b]	IS[c]	AS[d]
10	4.85	> 1000[e]	360 ± 34	41 ± 6
5	6.30	770 ± 60	210 ± 29	20 ± 2
11	7.81	2500 ± 120	150 ± 3	96 ± 14

[a] K_i values reflect the inhibition with respect to chorismate. [b] Each inhibitor competitively inhibited chorismate and Mg^{2+}. [c] Each inhibitor displayed competitive inhibition versus chorismate and noncompetitive inhibition versus Mg^{2+}. [d] Each inhibitor displayed mixed inhibition versus chorismate and competitively inhibited Mg^{2+}. [e] No inhibition was observed up to 1000 μM; assaying above 1000 μM was not possible due to instrument and assay limitations.

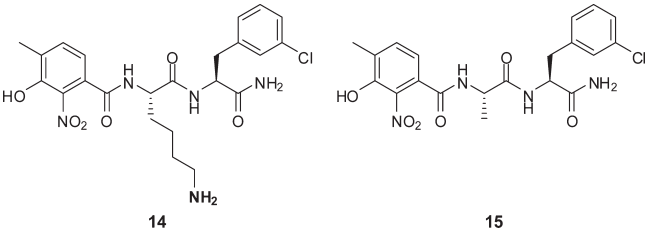

Figure 12. COMBI+SPACER (**14**) and COMBI-only (**15**) compounds were synthesized and assayed against ADCS, IS, and AS to verify that the PAYLOAD directs the inhibitors to the active site and that all three stages are necessary for optimal inhibition.

inhibitors **3**–**9** to the active site, only insofar as one can consider magnesium's binding site the active site.

Two possibilities can explain the competitive inhibition of IS by PAYLOAD-deleted **14** and **15**. In the first possibility, the COMBI stages of **14** and **15** only bind to IS when chorismate is absent, in the same manner as the fully staged inhibitors (e.g., **3**–**9**), and prevent chorismate binding. IS undergoes a much smaller conformational change on chorismate binding and, by extension, PAYLOAD binding (Figure 5), compared to ADCS. Therefore, the surface residues of IS are more similar in orientation in the unbound and PAYLOAD-bound forms. This would favor COMBI-SPACER-only **14** and COMBI-only **15** binding to the same region of IS as do the COMBI elements of fully staged inhibitors. In the second possibility, the COMBI stage of **14** and **15** interact with IS in a fundamentally different manner than in the fully staged inhibitors. If the first is correct, then the optimal binding mode for the COMBI stage alone (i.e., **14** and **15**) is that observed for the fully staged inhibitor. If the second is correct, then the PAYLOAD stage enforces a specific binding mode for the COMBI stage that is suboptimal but nevertheless enhances overall binding.

Table 4. Validation of PAYLOAD-Directed Active Site Binding to ADCS, IS, and AS

	ADCS		IS		AS	
inhibitor	K_i (μM)	mode	K_i (μM)	mode	K_i (μM)	mode
5	770 ± 60	C[a]	210 ± 29	C[a,b]	20 ± 2	N−C[c,d]
14	5700 ± 1000	N−C[b,c]	790 ± 88	C[a,b]	110 ± 6	N−C[b,c]
15	6800 ± 2000	N−C[b,c]	500 ± 72	C[a,b]	200 ± 11	N−C[b,c]

[a] C denotes competitive inhibition with respect to chorismate. [b] Noncompetitive inhibition with respect to Mg^{2+} was exhibited. [c] N−C denotes noncompetitive inhibition with respect to chorismate. [d] Competitive inhibition with respect to Mg^{2+} was observed.

The present work is a major step toward realization of our goal to find a single, potent compound that inhibits multiple

chorismate-utilizing enzymes. The inhibition results presented in Tables 2−4 validate the design approach: lysine was the correct choice as SPACER; the inhibitors are directed to the active site of ADCS by the PAYLOAD; all three stages are necessary for optimal inhibition. Five compounds (**3**, **5**−**7**, **9**) display low- to midmicromolar inhibition of three enzymes. Considering that these compounds were discovered in an ADCS on-bead screen, the fact that better inhibition is observed against IS and AS is remarkable.

The AS inhibition results presented in Tables 2−4 are more difficult to interpret due to the noncompetitive inhibition of chorismate binding by **1**−**9**. It will be necessary to optimize the PAYLOAD such that it competitively inhibits chorismate binding before going forward with future library syntheses. Concurrent with our original report of this peptide-based library, others reported low micromolar inhibition of AS by 1-carboxyethoxy-containing aromatic acids.[23,24] Among the reported chorismate analogues, the very simple analogue **1** was chosen to serve as the PAYLOAD in the present work because it was best suited for solid phase synthesis (e.g., compound stability, lack of stereocenters, pliant protecting group requirements, synthetic accessibility, etc.) in this small, proof-of-concept library. The next phase of this project is to move to larger, nonpeptide based libraries with more drug-like properties. Future efforts will employ the more potent 1-carboxyethoxy-containing PAYLOAD. If COMBI elements in future nonpeptide based libraries can improve binding by a modest factor of 40 (as demonstrated for **5** against IS) and if the PAYLOAD has a low micromolar K_i,[23,24] discovery of fully staged, multienzyme inhibitors with low- to midnanomolar inhibition is a realistic goal with unique therapeutic potential.

Experimental Procedures

Materials. All reagents and solvent that were purchased from commercial suppliers were used without further purification. Triethanolamine (TEA), bicine, KCl, HCl, NaOH, $(NH_4)_2SO_4$, KH_2PO_4, K_2HPO_4, $MgCl_2$, glacial acetic acid (AcOH), acetonitrile (ACN), ethylenediaminetetraacetate (EDTA), and L-glutamine, were purchased from Fisher. Pyridoxal 5′-phosphate (PLP), dithiothreitol (DTT), nicotinamide adenine dinucleotide, reduced form (NADH), lysozyme, anthranilic acid, and 2-mercaptoethanol were purchased from Sigma-Aldrich. The enzymes lactate dehydrogenase (LDH) and DNase I were purchased from Roche. Chorismate was prepared according to a literature procedure.[25] Fmoc rink amide-MBHA resin (capacity, 0.59 mmol/g; MBHA, 4-methylbenzhydrylamine; Fmoc, 9*H*-fluoren-9-ylmethoxycarbonyl) was purchased from Hecheng Science and Technology Co., Ltd., and all calculations for the synthesis were based on a substitution of 0.59 mmol/g. Fmoc-3-chloro-L-phenylalanine was purchased from Chem-Impex International, Inc. Fmoc-Ala-OH, Fmoc-Lys(Dde)-OH, Fmoc-Orn(Dde)-OH, and Fmoc-OSu were purchased from Novabiochem. The coupling reagents, HOBt and DIC, were purchased from AK Scientific. All other synthetic reagents and solvents were purchased from Sigma-Aldrich. Compound **13** was prepared according to literature procedures.[26−29] All infrared spectra were determined on a Genesis II Mattson FT-IR spectrometer. ^1H and ^{13}C NMR were measured in DMSO-d_6 at 600 MHz. Preparative high performance liquid chromatography (HPLC) was performed on a Waters system (2487 dual wavelength absorbance detector, 600 controller, and a 2767 sample manager) with the following specifications: electrospray (+) ionization (ESI), mass range 150−1500 Da, 20 V cone voltage, and Xterra MS C_{18} column (2.1 mm × 50 mm × 3.5 μm). High-resolution mass spectral (HRMS) data was acquired on a Thermo Fisher LTQ Orbitrap mass spectrometer (San Jose, CA) by flow-injection analysis in the positive ion mode using the IonMax electrospray source with 0.1% formic acid and methanol (MeOH) as the mobile phases. The source voltage was 5.5 kV, sheath gas setting of 8, and capillary temperature of 250 °C. Compounds synthesized here were confirmed to be 95+% pure by LC-MS under the conditions described above.

Enzyme Preparation. The plasmid construct bearing the genes for the partial complex of anthranilate synthase ($TrpE_2TrpG_2$) was a generous gift from Professor Ronald Bauerle, University of Virginia. Partial complex anthranilate synthase (AS) from *Salmonella typhimurium* consists of two TrpE:TrpG heterodimers. Plasmid pSTS23 contains two tandem stop codons engineered into the *trpD* gene, such that only the region encoding amidotransferase activity is expressed; the polypeptide translated from this truncated gene is named TrpG.[30]

AS was prepared in the following manner: *Escherichia coli* cells (strain CB694) harboring the pSTS23 construct were grown in luria-bertani broth (LB) media at 37 °C to an OD_{600} of 2.5−3. Cells were harvested by centrifugation and resuspended in lysis buffer (10 mM TEA, pH 7.8, 10 mM mercaptoethanol, 5 mM $MgCl_2$, 1 mM EDTA, 0.5 mg/mL lysozyme, 0.2 units/mL DNase I) prior to disruption by sonication. Cell debris was pelleted by centrifugation at 14000 rpm. Ammonium sulfate (23%) was added to the soluble extract; the resulting precipitate was resuspended in a minimum volume of start buffer (10 mM TEA, pH 7.8, 10 mM mercaptoethanol, 5 mM $MgCl_2$, 1 mM EDTA) and loaded onto Q-Sepharose Fast Flow (Pharmacia) resin. Protein was eluted with a linear gradient of 500 mL of 0−300 mM KCl in starting buffer. The purest fractions, as judged by sodium dodecyl sulfate polyacrylamide gel electrophoresis (SDS-PAGE) analysis, were concentrated by ultrafiltration and dialyzed against 20 mM KP_i pH 7.5, 50 mM KCl, 1 mM DTT. Purified enzyme was flash-frozen and stored at −80 °C. Protein concentration was measured with the Lowry protein assay kit (Bio-Rad) using IgG as standard. Yield was ∼142 mg purified protein/10 g cell paste.

The *entB* gene encoding isochorismatase (EntB) was amplified from *E. coli* K12 genomic DNA. The PCR primers were designed to introduce *NdeI* and *XhoI* restriction sites into the PCR products. The sequences of the primers used were: 5′-GGAATTCCATATGGCTATTCCAAAATTACA-3′ (forward) and 5′-CCCCTCGAGTCATTATTTCACCTCGCGGGAG-AG-3′ (reverse). PCR products of Taq DNA polymerase were cloned into the pCR2.1-TOPO vector using the TOPO TA Cloning kit (Invitrogen). Clones containing *entB* inserts were identified and isolated by blue−white screening and were subsequently subcloned into the pET28a vector (Novagen) using *NdeI* and *XhoI* restriction sites for expression as a 6xHis-tagged fusion protein.

BL21(DE3) *E. coli* cells harboring the pET28a-entB construct were grown in LB media at 37 °C to an OD_{600} of 0.6. Overexpression proceeded for six hours at 37 °C following induction by 0.5 mM β-isopropylthiogalactoside (IPTG). Cells were harvested by centrifugation and resuspended in lysis buffer (20 mM Na_2HPO_4, 500 mM NaCl, 10 mM imidazole, pH 7.4, 0.5 mg/mL lysozyme, 0.2 units/mL DNase I) prior to disruption by sonication. Cell debris was pelleted by centrifugation at 14000 rpm for 45 min. The supernatant was incubated at 4 °C for 45 min with Chelating Sepharose Fast Flow resin (Pharmacia) that had been charged with Ni^{2+}. The resin was loaded into a column and washed with 10 column volumes of starting buffer (20 mM Na_2HPO_4, 500 mM NaCl, 10 mM imidazole, pH 7.4). Protein was eluted with a linear gradient of 500 mL of 10−300 mM imidazole in starting buffer. The purest fractions, as judged by SDS-PAGE analysis, were concentrated by ultrafiltration and dialyzed against 20 mM KP_i pH 7.5, 50 mM KCl, 1 mM DTT. Purified enzyme was flash-frozen and stored at −80 °C.

Protein concentration was measured with the Lowry protein assay kit (Bio-Rad) using IgG as standard. Yield was ~350 mg purified protein/28 g cell paste.

IS was expressed from a pET28a-entC construct[31] and purified from BL21 (DE3) *E. coli* cells harboring the pET28a-*entC* plasmid construct according to a literature procedure,[31] which is similar to that described above for EntB. Protein yield was 213 mg/42 g cell paste.

Preparation of the plasmid constructs bearing the genes for PabA, PabB, and ADCL was described previously.[32] Protein expression and purification of these three enzymes followed literature procedures.[32] Protein yields were as follows: 83 mg PabA/15 g cell paste; 330 mg ADCS/20 g cell paste; 466 mg ADCL/37 g cell paste.

Spectrofluorometric AS Activity Assay. All kinetic assays were performed on a PerkinElmer LS 50B luminescence spectrophotometer at 25 °C. The activity assay for AS was based on a previously described method.[30] The assay directly monitors anthranilate emission at 390 nm using excitation at 313 nm. Reactions were initiated by addition of anthranilate synthase following a 5 min incubation at 25 °C. Each 1 mL reaction consisted of 100 mM phosphate buffer, pH 7.0, 20 mM L-glutamine, 5 mM $MgCl_2$, and 2.2 nM AS.

Spectrophotometric IS and ADCS Activity Assays. Kinetic assays were performed on either a Kontron Uvikon 930 or a Shimadzu UV-2450 UV−vis spectrophotometer at 25 °C. The activity assay for IS was described previously.[31] Formation of isochorismate was monitored at 278 nm ($\Delta\varepsilon_{\text{isochorismate-chorismate}}$ = 10211 M^{-1} cm^{-1}).[33] Each 1 mL reaction consisted of 50 mM triethanolamine, pH 7.8, 1 mM $MgCl_2$, and 50 nM IS. Reaction mixtures were incubated for 5 min at 25 °C prior to initiation with IS.

ADCS activity was monitored by following the decrease in absorbance at 340 nm, due to oxidation of NADH in a coupled assay with excess LDH and ADCL. Each 0.5 mL reaction contained 0.1 M bicine, pH 8.5, 0.02 M L-glutamine, 5 mM $MgCl_2$, 20 μM PLP, 100 μM NADH, 8 μM ADCL, 2 units LDH, 0.5 μM PabA, and 0.5 μM PabB. Reaction mixtures were incubated for 5 min at 25 °C prior to initiation with an equimolar solution of PabA and PabB. The rate of 4-amino-4-deoxychorismate (ADC) formation was confirmed to be linearly dependent on PabB concentration in the coupled assay.

Inhibition Assays and K_i Determination. Because of strong absorbance at 278 nm by the inhibitors, the IS activity assay described above was incompatible as an inhibition assay. Therefore, inhibition data was acquired by measuring initial rates in a coupled assay with excess EntB and LDH enzymes. The decrease in absorbance at 340 nm due to oxidation of NADH was monitored. Each 0.9 mL reaction contained 50 mM triethanolamine, pH 7.8, 1 mM $MgCl_2$, 100 μM NADH, 2 μM EntB, 2 units LDH, and 75 nM IS. The rate of isochorismate formation was confirmed to be linearly dependent on IS concentration in this coupled assay. The AS inhibition assay is the same as that described above; ADCS inhibition data was collected spectrophotometrically using the ADCL-LDH coupled assay described above.

Inhibitors were dissolved in water and brought to pH 8.5 with 25 mM NaOH. Inhibitor concentrations were varied from 10 μM to 8 mM, chorismate concentration was varied from 0.5 to 5 K_M, and magnesium concentration was saturating (e.g., 1 mM for IS reactions, 5 mM for ADCS and AS reactions). To determine the inhibition pattern with respect to magnesium, Mg^{2+} concentration was varied from 5 to 500 μM, and chorismate concentration was saturating (e.g., 200 μM for IS and ADCS reactions, 40 μM for AS reactions). K_i values were determined by globally fitting the data to competitive (eq 2), noncompetitive (eq 3), and mixed (eq 4) kinetic equations via the software program GraFit, Version 4.0.21 (Erithacus). Reported K_i values are from the best global fit, as determined by nonlinear regression analysis.

$$v_i = \frac{V_{max}[\text{chorismate}]}{K_M\left(\frac{[I]}{K_i}\right) + [\text{chorismate}]} \quad (2)$$

$$v_i = \frac{V_{max}[\text{chorismate}]}{K_M\left(1+\frac{[I]}{K_i}\right) + [\text{chorismate}]\left(1+\frac{[I]}{K_i}\right)} \quad (3)$$

$$v_i = \frac{V_{max}[\text{chorismate}]}{K_M\left(1+\frac{[I]}{K_i}\right) + [\text{chorismate}]\left(1+\frac{[I]}{\alpha K_i}\right)} \quad (4)$$

Inhibitor Synthesis and Characterization. Synthesis of 2-(3-(-(*S*)-5-((*S*)-1-Amino-3-(3-chlorophenyl)-1-oxopropan-2-ylamino)-4-(3-hydroxy-4-methyl-2-nitrobenzamido)-5-oxopentylcarbamoyl)-phenoxy)acetic Acid (10). Rink amide MBHA (1 g, 0.59 mmol/g loading capacity) resin was weighed into a plastic column and swollen in dimethylformamide (DMF) for 2 h, after which the DMF was drained, 20% piperidine in DMF was added to the resin, and the column was placed on a shaker for 2 × 10 min. After the resin was washed (DMF 2×, MeOH 2×, dichloromethane (DCM) 2×, MeOH 2×, and DMF 2×), Fmoc-3-chloro-L-phenylalanine (3.0 equiv) and HOBt (5.0 equiv) were premixed in dry DMF (10 mL) and added to the resin, followed by addition of diisopropylcarbodiimide (DIC) (5.0 equiv). The column was placed on a shaker until the Kaiser test was negative (~4 h). The resin was washed according to the procedure outlined above and the Fmoc group was removed. Following the standard wash, Fmoc-L-Orn(Dde)-OH (3.0 equiv) and *n*-hydroxybenzotriazole (HOBt) (5.0 equiv) were dissolved in DMF and added to the resin, with subsequent addition of DIC (5.0 equiv). The column was placed on a shaker until the Kaiser test was negative. The resin was washed, followed by Fmoc-deprotection standard conditions. After the resin was washed, a solution of 3-hydroxy-4-methyl-2-nitrobenzoic acid (3.0 equiv) and HOBt (5.0 equiv) in DMF were added to the resin followed by addition of DIC (5.0 equiv). The column was placed on a shaker until the Kaiser test was negative. After the wash, the 1-(4,4-dimethyl-2,6-dioxocyclohexylidene)ethyl (Dde) group was removed by addition of hydrazine (2% in DMF, 2 × 10 min). The resin was washed, and a DMF solution of 3-(2-*tert*-butoxy-2-oxoethoxy)benzoic acid (3.0 equiv), and HOBt (5.0 equiv) was added, followed by addition of DIC (5.0 equiv). The resin was washed and a cleavage mixture of trifluoroacetic acid (TFA), H_2O, and triisopropylsilane (TIS) (95:2.5:2.5, v/v/v) was added. The column was placed on a shaker for 2 h, and the filtrate was drained and collected. The TFA was evaporated under a constant stream of nitrogen, and the resulting residue was precipitated from ether and stored in the refrigerator overnight. The ether-crude mixture was centrifuged and the ether decanted. The crude mixture was purified by reversed-phase HPLC (630 mg, 63% yield, purity >99%); mp 154−156 °C. IR (thin film, selected peaks): ν 3266, 1637, 1124, 1324, 1229, 1020, 685 cm^{-1}. HRMS (ESI) m/z $[M+H]^+$ calculated for $C_{31}H_{33}ClN_5O_{10}$: 670.1916; found 670.1909. ^{1}H NMR (DMSO, 600 MHz): δ 13.01 (br s, 1 H), 10.06 (s, 1 H), 8.64 (d, 1 H, J = 7.8 Hz), 8.43 (t, 1 H, J = 5.4 Hz), 7.94 (d, 1 H, J = 8.4 Hz), 7.45−7.05 (m, 12 H), 4.72 (s, 2 H), 4.45 (m, 1 H), 4.32 (m, 1 H), 3.24 (m, 2 H), 3.01 (dd, 1 H, J = 13.8, 5.4 Hz), 2.83 (dd, 1 H, J = 13.8, 9.0 Hz), 2.27 (s, 3 H), 1.70−1.46 (m, 4 H). ^{13}C NMR (DMSO-d_6, 150 MHz): δ 172.4, 171.1, 170.1, 165.7, 164.3, 157.6, 147.1, 140.3, 139.5, 136.0, 132.7, 131.8, 131.3, 129.8, 129.4, 129.0, 128.0, 127.3, 126.3, 119.9, 119.0, 117.3, 113.1, 64.5, 53.4, 53.2, 38.9, 37.3, 29.2, 25.8, 16.5.

Synthesis of 2-(3-(3-((*R*)-3-((*S*)-1-Amino-3-(3-chlorophenyl)-1-oxopropan-2-ylamino)-2-(3-hydroxy-4-methyl-2-nitrobenzamido)-3-oxopropylthio) propylcarbamoyl)phenoxy)acetic Acid (11). A procedure identical to that described for **10** was followed, with the exception that compound **13** was used instead of

Fmoc-L-Orn(Dde)-OH. Therefore, removal of the Dde group was not necessary, nor was addition of 3-(2-*tert*-butoxy-2-oxoethoxy)-benzoic acid. The crude mixture was purified by reversed-phase HPLC (27 mg, 31% yield, purity >99%); mp 168−170 °C. IR (neat, selected peaks): 3266, 16.38, 1580, 1543, 1532 cm^{-1}. HRMS (ESI) *m*/*z* $[M + H]^+$ calcd for $C_{32}H_{34}ClN_5O_{10}S$: 716.1793; found 716.1864. ^1H NMR (DMSO-d_6): δ 13.05 (s, 1H), 10.09 (s, 1H), 8.72 (dd, J = 8.2, 1H), 8.47 (s, 1H), 8.14 (d, J = 8.2, 1H), 7.44−7.36 (m, 5H), 7.28 (s, 1H), 7.23 (d, J = 5.4, 2H), 7.21−7.12 (m, 3H), 7.06 (d, J = 8.2, 1H), 4.72 (s, 2H), 4.48 (m, 2H), 3.31 (s, 2H), 3.03 (m, 1H), 2.89−2.77 (m, 2H), 2.77−2.64 (m, 1H), 2.64−2.54 (m, 2H), 2.27 (s, 3H), 1.75 (m, 2H). ^{13}C NMR (DMSO-d_6): δ 172.9, 170.7, 170.4, 166.4, 164.6, 158.3, 147.6, 140.9, 140.3, 136.4, 133.3, 132.4, 132.0, 130.0, 129.7, 129.6, 128.7, 127.4, 127.0, 120.6, 119.7, 117.9, 113.3, 65.1, 54.3, 53.6, 38.9, 37.8, 33.7, 29.7, 29.4, 17.2.

Synthesis of *N*-((*S*)-6-Amino-1-((*S*)-1-amino-3-(3-chlorophenyl)-1-oxopropan-2-ylamino)-1-oxohexan-2-yl)-3-hydroxy-4-methyl-2-nitrobenzamide (14). A procedure identical to that described for **10** was followed, with the exception that Fmoc-L-Lys(Dde)-OH was used instead of Fmoc-L-Orn(Dde)-OH and the addition of a DMF solution of 3-(2-*tert*-butoxy-2-oxoethoxy)-benzoic acid (3.0 equiv), and HOBt (5.0 equiv), followed by addition of DIC (5.0 equiv) was not performed after the Dde deprotection step. The crude mixture was purified by reversed-phase HPLC (212 mg, 71% yield, purity >99%); mp 134−135 °C. IR (neat, selected peaks): 2358, 2314, 1683, 1647, 1635, 1544 cm^{-1}. HRMS (ESI) *m*/*z* $[M + H]^+$ calculated for $C_{23}H_{28}ClN_5O_6$: 506.1806; found 506.1832. ^1H NMR (DMSO-d_6): δ 10.14 (s, 1H), 8.62 (d, J = 8.1, 1H), 7.94 (d, J = 8.2, 1H), 7.72 (s, 3H), 7.45 (s, 1H), 7.39 (d, J = 8.5, 1H), 7.28 (d, J = 7.2, 1H), 7.27−7.23 (m, 2H), 7.19 (d, J = 6.8, 1H), 7.14 (s, 1H), 4.51−4.41 (m, 1H), 4.28 (d, J = 5.2, 1H), 3.04 (dd, J = 4.9, 13.8, 1H), 2.84 (dd, J = 9.1, 13.8, 1H), 2.75−2.74 (m, 2H), 2.29 (s, 3H), 1.69−1.44 (m, 4H), 1.26 (s, 2H). ^{13}C NMR (DMSO-d_6): δ 172.9, 171.5, 165.1, 148.0, 140.9, 140.0, 133.4, 129.7, 128.7, 128.4, 126.8, 126.2, 119.9, 119.8, 105.0, 54.0, 40.5, 37.8, 31.9, 27.2, 22.9, 17.0, 16.9.

Synthesis of *N*-((*S*)-1-((*S*)-1-Amino-3-(3-chlorophenyl)-1-oxopropan-2-ylamino)-1-oxopropan-2-yl)-3-hydroxy-4-methyl-2-nitrobenzamide (15). A procedure identical to that described for **14** was followed, with the exception that Fmoc-L-Ala-OH was used instead of Fmoc-L-Lys(Dde)-OH; therefore, the Dde deprotection was not performed. The crude mixture was purified by reversed-phase HPLC (38 mg, 30% yield, purity >99%); mp 240−242 °C. IR (neat, selected peaks): 3274, 2969, 2358, 1642, 1545, 1418, 1478 cm^{-1}. HRMS (ESI) *m*/*z* $[M + H]^+$ calculated for $C_{20}H_{21}ClN_4O_6$: 449.1228; found 449.1267. ^1H NMR (DMSO-d_6): δ 10.04 (s, 1H), 8.63 (d, J = 7.3, 1H), 7.89 (d, J = 8.2, 1H), 7.35 (d, J = 7.8, 2H), 7.20−7.25 (m, 3H), 7.11−7.16 (m, 3H), 4.38 (dd, J = 8.6, 13.4, 1H), 4.28 (t, J = 7.2, 1H), 2.99 (dd, J = 4.9, 13.8, 1H), 2.81 (dd, J = 8.8, 13.8, 1H), 2.25 (s, 3H), 1.19 (d, J = 7.1, 1H). ^{13}C NMR (DMSO-d_6): δ 173.1, 172.3, 164.7, 147.8, 141.1, 140.2, 133.3, 132.5, 132.0, 130.5, 129.7, 128.7, 127.7, 126.9, 119.8, 54.1, 49.7, 37.7, 18.3, 17.2.

The synthesis of compounds **1**−**9** has been described previously.[5]

Acknowledgment. M.J.K. acknowledges support of this work from the National Science Foundation (CHE-0910870).

Supporting Information Available: Proton and carbon NMR spectra for compounds **10**, **11**, **14**, and **15**. This material is available free of charge via the Internet at http://pubs.acs.org.

References

(1) Coates, A.; Hu, Y.; Bax, R.; Page, C. The future challenges facing the development of new antimicrobial drugs. *Nat. Rev. Drug Discovery* **2002**, *1*, 895–910.
(2) Klevens, R. M.; Morrison, M. A.; Nadle, J.; Petit, S.; Gershman, K.; Ray, S.; Harrison, L. H.; Lynfield, R.; Dumyati, G.; Townes, J. M.; Craig, A. S.; Zell, E. R.; Fosheim, G. E.; McDougal, L. K.; Carey, R. B.; Fridkin, S. K. Invasive methicillin-resistant *Staphylococcus aureus* infections in the United States. *JAMA, J. Am. Med. Assoc.* **2007**, *298*, 1763–1771.
(3) Jarvis, L. M. An Uphill Battle. *Chem. Eng. News* **2008**, *86*, 15–20.
(4) Fischbach, M. A.; Walsh, C. T. Antibiotics for Emerging Pathogens. *Science* **2009**, *325*, 1089–1093.
(5) Dixon, S.; Ziebart, K. T.; He, Z.; Jeddeloh, M.; Yoo, C. L.; Wang, X.; Lehman, A.; Lam, K. S.; Toney, M. D.; Kurth, M. J. Aminodeoxychorismate synthase inhibitors from one-bead one-compound combinatorial libraries: "staged" inhibitor design. *J. Med. Chem.* **2006**, *49*, 7413–7426.
(6) Roberts, F.; Roberts, C. W.; Johnson, J. J.; Kyle, D. E.; Krell, T.; Coggins, J. R.; Coombs, G. H.; Milhous, W. K.; Tzipori, S.; Ferguson, D. J.; Chakrabarti, D.; McLeod, R. Evidence for the shikimate pathway in apicomplexan parasites. *Nature* **1998**, *393*, 801–805.
(7) Morphy, R.; Rankovic, Z. Designed multiple ligands. An emerging drug discovery paradigm. *J. Med. Chem.* **2005**, *48*, 6523–6543.
(8) Morphy, R.; Kay, C.; Rankovic, Z. From magic bullets to designed multiple ligands. *Drug Discovery Today* **2004**, *9*, 641–651.
(9) Weber, G.; Prajda, N.; Lui, M. S.; Denton, J. E.; Aoki, T.; Sebolt, J.; Zhen, Y. S.; Burt, M. E.; Faderan, M. A.; Reardon, M. A. Multienzyme-targeted chemotherapy by acivicin and actinomycin. *Adv. Enzyme Regul.* **1982**, *20*, 75–96.
(10) Hibasami, H.; Maekawa, S.; Murata, T.; Nakashima, K. Antitumor effect of a new multienzyme inhibitor of polyamine synthetic pathway, methylglyoxal-bis(cyclopentylamidinohydrazone), against human and mouse leukemia cells. *Cancer Res.* **1989**, *49*, 2065–2068.
(11) Zhan, P.; Liu, X. Y. Designed Multiple Ligands: An Emerging Anti-HIV Drug Discovery Paradigm. *Curr. Pharm. Des.* **2009**, *15*, 1893–1917.
(12) Arora, P.; Goyal, A.; Natarajan, V. T.; Rajakumara, E.; Verma, P.; Gupta, R.; Yousuf, M.; Trivedi, O. A.; Mohanty, D.; Tyagi, A.; Sankaranarayanan, R.; Gokhale, R. S. Mechanistic and functional insights into fatty acid activation in *Mycobacterium tuberculosis*. *Nat. Chem. Biol.* **2009**, *5*, 166–173.
(13) Barkan, D.; Liu, Z.; Sacchettini, J. C.; Glickman, M. S. Mycolic Acid Cyclopropanation is Essential for Viability, Drug Resistance, and Cell Wall Integrity of *Mycobacterium tuberculosis*. *Chem. Biol.* **2009**, *16*, 499–509.
(14) Chen, J. K.; Lane, W. S.; Brauer, A. W.; Tanaka, A.; Schreiber, S. L. Biased combinatorial libraries: Novel ligands for the SH3 domain of phosphatidylinositol 3-kinase. *J. Am. Chem. Soc.* **1993**, *115*, 12591–12592.
(15) Sternson, S. M.; Wong, J. C.; Grozinger, C. M.; Schreiber, S. L. Synthesis of 7200 small molecules based on a substructural analysis of the histone deacetylase inhibitors trichostatin and trapoxin. *Org. Lett.* **2001**, *3*, 4239–4242.
(16) Erlanson, D. A. Fragment-based lead discovery: a chemical update. *Curr. Opin. Biotechnol.* **2006**, *17*, 643–652.
(17) Parsons, J. F.; Jensen, P. Y.; Pachikara, A. S.; Howard, A. J.; Eisenstein, E.; Ladner, J. E. Structure of *Escherichia coli* aminodeoxychorismate synthase: architectural conservation and diversity in chorismate-utilizing enzymes. *Biochemistry* **2002**, *41*, 2198–2208.
(18) Spraggon, G.; Kim, C.; Nguyen-Huu, X.; Yee, M. C.; Yanofsky, C.; Mills, S. E. The structures of anthranilate synthase of *Serratia marcescens* crystallized in the presence of (i) its substrates, chorismate and glutamine, and a product, glutamate, and (ii) its end-product inhibitor, L-tryptophan. *Proc. Natl. Acad. Sci. U.S.A* **2001**, *98*, 6021–6026.
(19) Morollo, A. A.; Eck, M. J. Structure of the cooperative allosteric anthranilate synthase from *Salmonella typhimurium*. *Nat. Struct. Biol.* **2001**, *8*, 243–247.
(20) Parsons, J. F.; Shi, K. M.; Ladner, J. E. Structure of isochorismate synthase in complex with magnesium. *Acta Crystallogr., Sect. D: Biol. Crystallogr.* **2008**, *64*, 607–610.
(21) Kolappan, S.; Zwahlen, J.; Zhou, R.; Truglio, J. J.; Tonge, P. J.; Kisker, C. Lysine 190 is the catalytic base in MenF, the menaquinone-specific isochorismate synthase from *Escherichia coli*: implications for an enzyme family. *Biochemistry* **2007**, *46*, 946–953.
(22) Segel, I. H. *Enzyme Kinetics: Behavior and Analysis of Rapid Equilibrium and Steady State Enzyme Systems*. Wiley: New York, 1975; pp xxii, 957.
(23) Payne, R. J.; Bulloch, E. M.; Abell, A. D.; Abell, C. Design and synthesis of aromatic inhibitors of anthranilate synthase. *Org. Biomol. Chem.* **2005**, *3*, 3629–3635.
(24) Payne, R. J.; Kerbarh, O.; Miguel, R. N.; Abell, A. D.; Abell, C. Inhibition studies on salicylate synthase. *Org. Biomol. Chem.* **2005**, *3*, 1825–1827.

(25) Grisostomi, C.; Kast, P.; Pulido, R.; Huynh, J.; Hilvert, D. Efficient in Vivo Synthesis and Rapid Purification of Chorismic Acid Using an Engineered *Escherichia coli* Strain. *Bioorg. Chem.* **1997**, *25*, 297–305.
(26) Ensch, C.; Hesse, M. Total syntheses of the spermine alkaloids (−)-(*R*,*R*)-hopromine and (±)-homaline. *Helv. Chim. Acta* **2002**, *85*, 1659–1673.
(27) Bolognese, A.; Fierro, O.; Guarino, D.; Longobardo, L.; Caputo, R. Chiral aminoalkyl cation equivalents. 1. One-pot synthesis of orthogonally protected enantiopure *S*-(aminoalkyl)cysteine derivatives. *Eur. J. Org. Chem.* **2005**, 169–173.
(28) Lopez, P. E.; Isidro-Llobet, A.; Gracia, C.; Cruz, L. J.; Garcia-Granados, A.; Parra, A.; Alvarez, M.; Albericio, F. Use of *p*-nitrobenzyloxycarbonyl (pNZ) as a permanent protecting group in the synthesis of Kahalalide F analogs. *Tetrahedron Lett.* **2005**, *46*, 7737–7741.
(29) Tietze, L. F.; Panknin, O.; Major, F.; Krewer, B. Synthesis of a novel pentagastrin−drug conjugate for a targeted tumor therapy. *Chem.—Eur. J.* **2008**, *14*, 2811–2818.
(30) Bauerle, R.; Hess, J.; French, S. Anthranilate synthase−anthranilate phosphoribosyltransferase complex and subunits of *Salmonella typhimurium*. *Methods Enzymol.* **1987**, *142*, 366–386.
(31) He, Z.; Toney, M. D. Direct detection and kinetic analysis of covalent intermediate formation in the 4-amino-4-deoxychorismate synthase catalyzed reaction. *Biochemistry* **2006**, *45*, 5019–5028.
(32) He, Z.; Stigers Lavoie, K. D.; Bartlett, P. A.; Toney, M. D. Conservation of mechanism in three chorismate-utilizing enzymes. *J. Am. Chem. Soc.* **2004**, *126*, 2378–2385.
(33) Morollo, A. A.; Bauerle, R. Characterization of composite aminodeoxyisochorismate synthase and aminodeoxyisochorismate lyase activities of anthranilate synthase. *Proc. Natl. Acad. Sci. U.S.A* **1993**, *90*, 9983–9987.